The upper crustal 3-D resistivity structure of the Kristineberg area, Skellefte district, northern Sweden revealed by magnetotelluric data

Juliane Hübert,* María de los Ángeles García Juanatey, Alireza Malehmir, Ari Tryggvason and Laust B. Pedersen

Department of Earth Sciences, Geophysics, Uppsala University, Villavägen 16, SE-752 36 *Uppsala, Sweden. E-mail: huebert@ualberta.ca*

SUMMARY

A 3-D model of the crustal electrical resistivity was constructed from the inversion of magnetotelluric data in the Kristineberg area, Skellefte district, the location of one of Sweden's most successful mining activities. Forward modelling of vertical magnetic transfer data supports our model which was derived from the magnetotelluric impedance only. The dominant features in the 3-D model are the strong conductors at various depth levels and resistive bodies of variable thickness occurring in the shallower subsurface. The deepest conductor, previously associated with the Skellefte crustal conductivity anomaly, is imaged in the southern part of the area as a north-dipping feature starting at ∼4 km depth. Several shallow conductors are attributed to graphite in the black shales defining the contact between the metasedimentary rocks and the underlying metavolcanic rocks. Furthermore, an elongated intermediate depth conductor is possibly associated with alteration zones in the metavolcanic rocks that host the ore occurrences. The most prominent crustal resistors occur in the southern and northern part of the area, where their lateral extent on the surface coincides with the late-orogenic Revsund type intrusions. To the east, a resistive feature can be correlated to the early-orogenic Viterliden intrusion. The 3-D model is compared with two previous 2-D inversion models along two perpendicular profiles. The main electrical features are confirmed with the new model and previous uncertainties regarding 3-D effects, caused by off-profile conductors, can be better assessed in 3-D, although the resolution is lower due to a coarser model discretization. The comparison with seismic sections along two north–south profiles reveals structural correspondence between electrical features, zones of different reflectivity and geological units.

Key words: Crustal structure; Electrical properties; Magnetotelluric.

1 INTRODUCTION

Complex geological structures have always been a challenge to 2-D magnetotelluric (2-D MT) inversion models. Forward modelling studies, for example, Muñoz *et al.* (2008), have illustrated the importance of 3-D conductivity models for an undistorted image of the composition and structure of the Earth's crust, even though the common practice of field setup and available inversion codes allowed only for 2-D conductivity models. The limitations of interpreting 3-D structures with 2-D MT have been observed and studied by, for example, Ledo *et al.* (2002) and Pedersen & Engels (2005), but only recent advances in algorithms (e.g. Newman & Alumbaugh 2000; Farquharson *et al.* 2002; Siripunvaraporn *et al.* 2005; Zhdanov *et al.* 2010) and affordable as well as expedient instrumentation have made it feasible to both measure and invert 3-D data sets. With these developments it is now possible to overcome

dimensionality issues in a variety of complex geological settings (e.g. Hautot *et al.* 2007; Arnason *et al.* 2010; Heise *et al.* 2010).

We present an example of integrating 3-D magnetotellurics into an interdisciplinary study, 'Vinnova 4D modelling of mineral belts'[1], that comprises both geophysical and geologic observations. The study area is located in the Palaeoproterozoic Skellefte district in northern Sweden, one of Europe's most productive mining areas. Our aim is to image the structure of the area with magnetotellurics in order to aid the assessment of the geological development of the whole district.

Over the last 3 years, a total of 67 broad-band magnetotelluric sites were installed in the area, mainly along one E–W oriented and three N–S profiles. As a first approach, 2-D inversion models were derived and interpreted (Hübert *et al.* 2009; García Juanatey *et al.* 2012). In this paper, we present a 3-D conductivity model of the whole Kristineberg area and assign lithological units to the observed

*Now at: Department of Earth and Atmospheric Sciences, University of Alberta, Edmonton, Canada T6G 2E3.
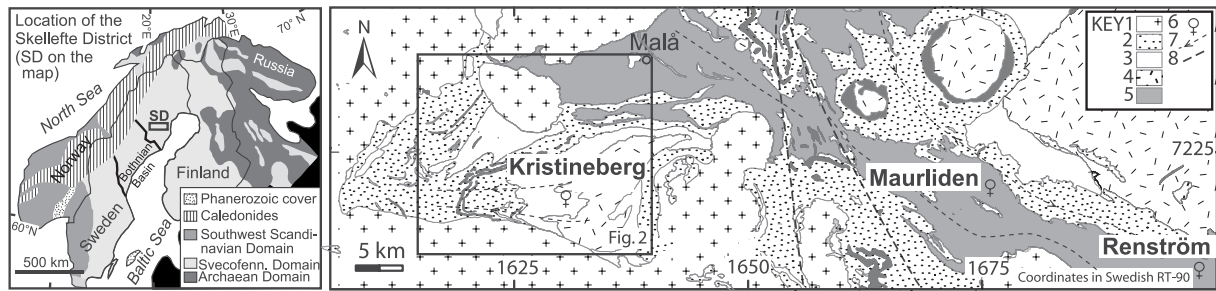
[1] http://www.ltu.se/research/subjects/Malmgeologi/Forskningsprojekt/4D-Modelling

Figure 1. Location of the Skellefte district, northern Sweden. Key: Left-hand side: geological overview of the Fennoscandian Shield. Right-hand side: geological sketch of the western part of the Skellefte District. (1) Late- to post-tectonic granites, (2) metasediments, (3) Skellefte Group metavolcanic rocks, (4) mafic intrusions (5) metagranitoids, (6) active mines, (7) axial trace of the main folds and (8) post-main deformation shear zones. Geology after Bergman-Weihed (1999–2000); Kathol & Weihed (2005).

electrical features. Previous uncertainties regarding the dimensionality of the data and the validation of the 2-D assumption are overcome with the inversion of the complete impedance tensor, although with a loss of resolution, in respect to the 2-D resistivity sections, in the final 3-D model. To examine the validity of the 3-D model, we performed forward modelling of the vertical magnetic transfer function (VMTF) and a detailed comparison with the 2-D result.

1.1 Geological background

The Skellefte District (see Fig. 1) in northern Sweden is known for its abundances in volcanic hosted massive sulphides (VHMS) mineral occurrences. It constitutes part of the Svecofennian province (*ca.* 1.90–1.8 Ga) and lies at the boundary between the domain of supracrustal rocks with reworked Archean rocks (Gaal & Gorbatshev 1987; Weihed *et al.* 1992; Rutland *et al.* 2001) to the north and the high-grade metamorphic (amphibolite facies) rocks of the Bothnian basin to the south. The latter consists largely of greywackes, gneisses and migmatites (Weihed *et al.* 1992; Bergström 2001). The supracrustal rocks in the western part of the Skellefte district (see Fig. 2) comprise (1) the Skellefte Group, a sequence dominated by subaqueous volcanic rocks (1.89–1.88 Ga, Skyttä *et al.* 2011), (2) the Vargfors Group dominated by shallow-water to sub-aerial sedimentary (1.88–1.87 Ga Billstrom & Weihed 1996; Bauer *et al.* 2011), (3) the Viterliden intrusion, ∼1.85 Ga, Skyttä *et al.* (2011) and (4) the postorogenic Revsund granite which belongs to the Transscandinavian igneous belt (1.82–1.78 Ga, Weihed *et al.* 2002). The origin of the basement is in debate. Tryggvason *et al.* (2006), Malehmir *et al.* (2006) and Hübert *et al.* (2009) have been suggesting a Bothnian Basin metasedimentary affinity based on the coincident presence of major north dipping reflectivities and a zone of high electrical conductivity. Due to a quite limited number of outcrops, the surface geology (see Fig. 2) is mainly defined with the support of airborne geophysical data (magnetic and Bouger gravity anomaly data provided by the Geological Survey of Sweden, see e.g. Malehmir *et al.* 2007).

The Kristineberg area, the focus of our study, is located in the Western Skellefte District (Årebäck *et al.* 2005; Skyttä *et al.* 2010). The main lithological units are metamorphic rocks of the Skellefte and Vargfors groups forming an anticline that is plunging to the west, cored by the Viterliden intrusion to the east and constrained by the intrusive rocks of the Revsund granite to the south, west and north, with an estimated maximum depth extent of about 3–4 km (Malehmir *et al.* 2009b).
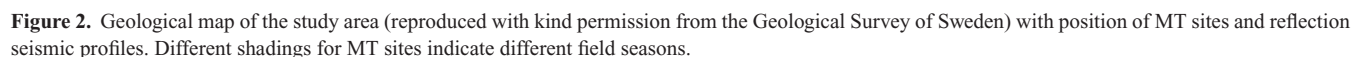
1.2 Previous geophysical studies

The Kristineberg area has been intensively investigated during recent years: A pilot study of geophysical investigations was launched

in 2003, including potential field modelling and two reflection seismic profiles (Tryggvason *et al.* 2006; Malehmir *et al.* 2007). One of the main findings was a group of strong and north dipping reflectors at 3–12 km depth that were interpreted as a possible thrust fault between the Skellefte volcanics and a sedimentary basement. A pilot 3-D geological model was presented by Malehmir *et al.* (2009b) including 3-D inverse gravity modelling and reflection seismic studies. A subsequent profile with broad band magnetotelluric measurements was collected in 2007 (Hübert *et al.* 2009) and led to a 2-D conductivity model that revealed a zone of high electrical conductivity coinciding with the north dipping reflector. To further study the Skellefte District, the Vinnova project '4D Modelling of mineral belts' was initiated in 2008, including the acquisition of two perpendicular reflection seismic (Dehghannejad *et al.* 2010) and MT profiles (García Juanatey *et al.* 2012). The new reflection seismic data allowed for another possible origin of the north dipping reflectors as a fault zone within the Viterliden intrusion instead of a lithological contrast. The MT data revealed the strong influence of a shallow highly conductive zone associated with black shales in the contact between the metavolcanic and metasedimentary units. Additionally, the presence of a strong conductivity anomaly at depth was confirmed. Furthermore, the geoelectrical properties of the Skellefte volcanics were portrayed as inhomogeneous. A strong diffraction pattern in the seismic reflection data from Profile 5 (Fig. 2) that apparently coincides with a zone of higher conductivity was investigated using 3-D crooked line techniques. Malehmir *et al.* (2009a) concluded that both resistivity and reflectivity anomalies could be caused by a zone of sheared and highly altered metavolcanic rocks.

2 MT DATA

The measurements were carried out during the field seasons of 2007–2010. Data coverage is mainly controlled by the limited accessibility of the Swedish forest and the presence of lakes and infrastructure (see Fig. 2). We used induction coil magnetometers MFS05/MFS06 from Metronix, Germany and LEMI from Lviv, Ukraine as well as non-polarizable Pb-PbCl electrodes. The temporal variations in the horizontal electric fields (e_x in north–south and e_y in east–west direction) and of all three components of the magnetic field (h_x, h_y, h_z) were recorded with a continuous sampling of 20 Hz for at least one day and a 2-hr local midnight time burst recording at 1000 Hz (not available at all sites). The signal strength due to solar activity increased from a low in 2007. However, the data quality was mainly controlled by the distance to infrastructure. Time series processing using both single site and remote reference techniques to estimate the magnetotelluric transfer function *Z* was carried out with the algorithms by Smirnov (2003). For the remote referencing, simultaneously recording sites in the survey area and a

Figure 2. Geological map of the study area (reproduced with kind permission from the Geological Survey of Sweden) with position of MT sites and reflection seismic profiles. Different shadings for MT sites indicate different field seasons.

remote site *ca.* 40 km away (only available during campaigns 2007 and 2008) were used. The complex impedance tensor *Z* is defined as the relation in frequency domain between the components of the magnetic field *H* and those of the electric field *E* measured at the surface of the Earth

$$\begin{bmatrix} E_x \\ E_y \end{bmatrix} = \begin{bmatrix} Z_{xx} & Z_{xy} \\ Z_{yx} & Z_{yy} \end{bmatrix} \cdot \begin{bmatrix} H_x \\ H_y \end{bmatrix} \qquad (1)$$

measured in magnetic north (*x*-direction) and east (*y*-direction). The quality of the data was varying, ranging from excellent along Profile 5 in the west to partly noisy close to the Kristineberg mine.

For a more detailed description of the data and dimensionality analysis in the area we refer to Hübert *et al.* (2009) and García Juanatey *et al.* (2012).

As these previous studies showed, it is difficult to determine a common geoelectrical strike direction along the profile lines that would be needed to satisfy the 2-D assumption. Where for Profile 5 a rather consistent strike direction of 75° could be determined and correlated with main geological contacts (Hübert *et al.* 2009), strike directions were ambiguous for the area west of the mine along the N–S and E–W Profile (García Juanatey *et al.* 2012). With the application of a 3-D inversion algorithm using the whole impedance tensor, it is now possible to overcome these inconsistencies.

3 3-D INVERSE MODELLING

With recent advances in available algorithms and a sufficient data coverage of the area it has become feasible to construct 3-D inversion models. These simulate the complete impedance tensor and are not dependent on any dimensionality assumptions. Due to the much larger computational costs and the high effort in collecting data in a 3-D grid the resolution of these models is reduced compared to 2-D models. We used the inversion code WSINV3DMT by Siripunvaraporn *et al.* (2005), which is a data space based occam-like minimum-structure inversion scheme that allows for the incorporation of the complete impedance tensor. The model space is discretized in a rectangular grid using the finite difference method. The model grid has $45 \times 45 \times 25$ cells in *x*, *y* and *z* direction, respectively. The cell size in the horizontal plane is 500×500 m (with growing cell sizes outside the space of observations), which ensured at least two cells between neighbouring stations to allow the inversion to compensate for local inhomogeneities that can be responsible for galvanic distortion of the data. Where necessary, the station positions were slightly shifted (<250 m) to reside in the middle of the cells. The minimum cell size in the vertical direction was set to 20 m to satisfy the condition that it should be smaller than the minimum skin depth in conductive regions (Siripunvaraporn *et al.* 2005). For an expected minimal resistivity of 1 Ωm the approximate skin depth is 40 m for the highest frequency in use (128 Hz). Out of the total number of 67 sites 42 were chosen, prioritizing good data quality and omitting too dense sampling in the 3-D grid. In addition to the real errors we applied different error floors of 5 and 10 per cent, calculated from the absolute value of a main impedance elements and applied also on the corresponding diagonal element ($\Delta Z_{xy} = \Delta Z_{xx}$ and $\Delta Z_{yx} = \Delta Z_{yy}$). Twelve periods between 128 Hz and 16 s were selected.

The inversion was run with different starting models: homogeneous half-spaces of 100 and 1000 Ωm as well as a layered starting model. The latter was derived from 1-D inversion of an averaged impedance over the whole array and contained three layers (with thickness $d_1 = 1$ km and resistivity 2000 Ωm; $d_2 = 1.5$ km, 10000 Ωm, $d_3 = 7$ km, 10 Ωm) over a half-space of 100 Ωm. Using a 1-D structure as the starting model did not result in improved models probably due to the presumed strong lateral changes in electrical resistivity especially in the centre of the investigation area. Different Lagrange and smoothing parameters were tested as well as different combinations of starting and prior models and error floors. The strategy was to start the inversion process with a set of parameters and starting/prior models until a reasonable model was achieved. This model was then used in a second step as the starting and prior model for another inversion run to further reduce rms data fit. The final and chosen model with an rms of 3.3 was accordingly derived with a homogeneous starting model of 1000 Ωm using an error floor of 10 per cent, the same smoothing in *x*-, *y*- and *z*-direction, a medium time step τ of 5 and the default Lagrange multiplier and step size. Examples of data and model responses for all impedance tensor elements of nine stations are displayed as scaled impedances (Fig. 3), which are similar to the more familiar representation of apparent resistivity ρ_a (*T*—period in seconds, μ_0—magnetic constant)

$$|Z'| = \frac{Z}{\sqrt{\frac{T}{2\pi\mu_0}}} \approx \sqrt{\rho_a}. \tag{2}$$

As the final rms of 3.3, although not ideal, is reasonable in comparison with other results using data from geological complex areas (e.g. Heise *et al.* 2008), the resulting model most likely represents the main geoelectrical structure of the Kristineberg area reasonably well and adds valid information to the existing 2-D interpretations.

3.1 Model assessment

The spatial distribution of the rms in the eight responses of the impedance as seen in Fig. 4 indicates that data fit in the central part of the area is the most problematic. Still, zones of worse fit are spread out in the responses and periods.

To ensure that the conductivity distribution in the final model was sufficiently discretized, the inversion was rerun with a denser grid ($55 \times 55 \times 45$ cells) with distinctively finer discretization in the vertical direction (starting with a cell size of 2 m). The resulting inversion model was very close to the one obtained with the coarser discretization, that is, it included the main electrical features and had a comparable rms. Therefore, in all subsequent tests the discretization was limited to the original setup. To test for the stability of the main model features, systematic forward modelling was performed. We excluded the conductors (shallow, intermediate and deep) from the final model and started another inversion to check if the data actually require their presence. The rms of the modified models from the forward calculation without the conductive structures were significantly higher. When used as starting models, the inversion introduces these features again. This is evidence that all the main conductive features in the model are required by the data.

The time consuming computation and limitations for including *a priori* information currently do not allow for a more thorough sensitivity analysis as was performed in 2-D (García Juanatey *et al.* 2012).

3.2 Forward modelling of the vertical magnetic transfer function

To further test the consistency of the derived conductivity model, we performed 3-D forward modelling of the vertical magnetic transfer function (VMTF) data. The VMTF, sometimes referred to as tipper, is the transfer function *T* between the vertical magnetic field H_z and the horizontal components H_x and H_y

$$H_z = \begin{bmatrix} T_x & T_y \end{bmatrix} \cdot \begin{bmatrix} H_x \\ H_y \end{bmatrix}. \tag{3}$$

The VMTF contains independent information about the conductivity structure of the subsurface and is usually incorporated in 2-D inverse modelling. However, this is not yet possible with the available 3-D inversion routine, so our evaluation of the VMTF data remains qualitative. Displayed as induction arrows, they give very instructive insights into the dimensionality of the underlying conductivity distribution. Following the Wiese convention (Wiese 1962) the arrows are pointing away from conductive structures. The measured VMTF data (see Fig. 5, left-hand panel) in the Kristineberg area is of varying quality both spatially and in the different frequency bands. Local conductivity anomalies can be identified within the higher frequencies, where the induction arrows in the central part point towards east and on Profile 5 mainly north or south. For longer periods a general north–northeast pointing trend for the whole array indicates a strong conductor to the south–southwest.

The forward modelling was performed with the algorithm *x3d* by Avdeev *et al.* (2002). This code uses an integral equation approach for the electromagnetic fields of both natural and artificial origin. The model is discretized in a rectangular mesh with increasing vertical layer thicknesses. The forward responses for three selected
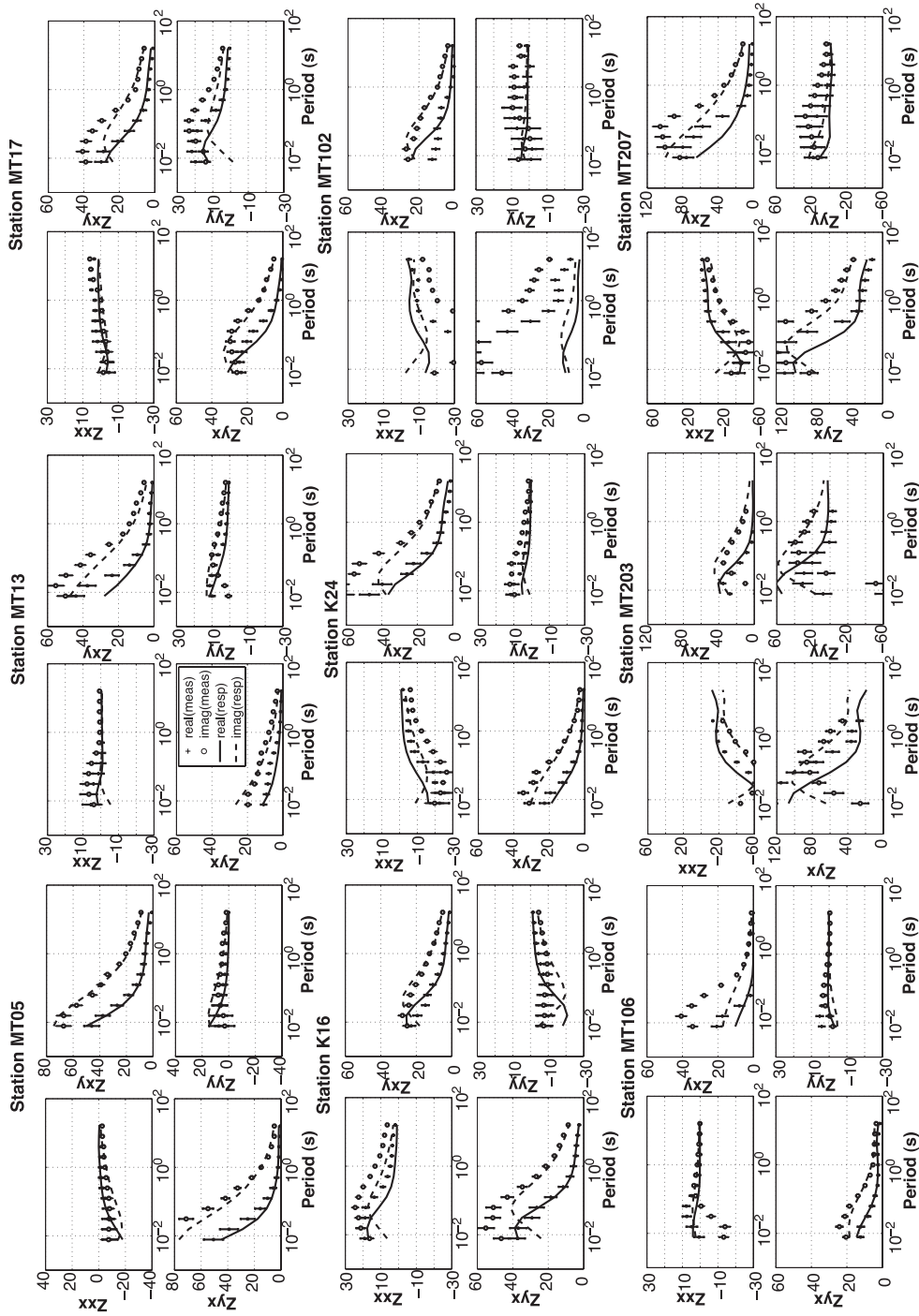
Figure 3. Comparison of observed and modelled data. Impedance tensor elements are scaled with $(\sqrt{\frac{T}{2\pi\mu_0}})^{-1}$. Measured data (circles for the real and crosses for the imaginary part respectively) with the errors used in inversion [max(error floor, original error)] and responses (solid lines) from the final model for a selection of the presented sites can be seen in Fig. 6(a).
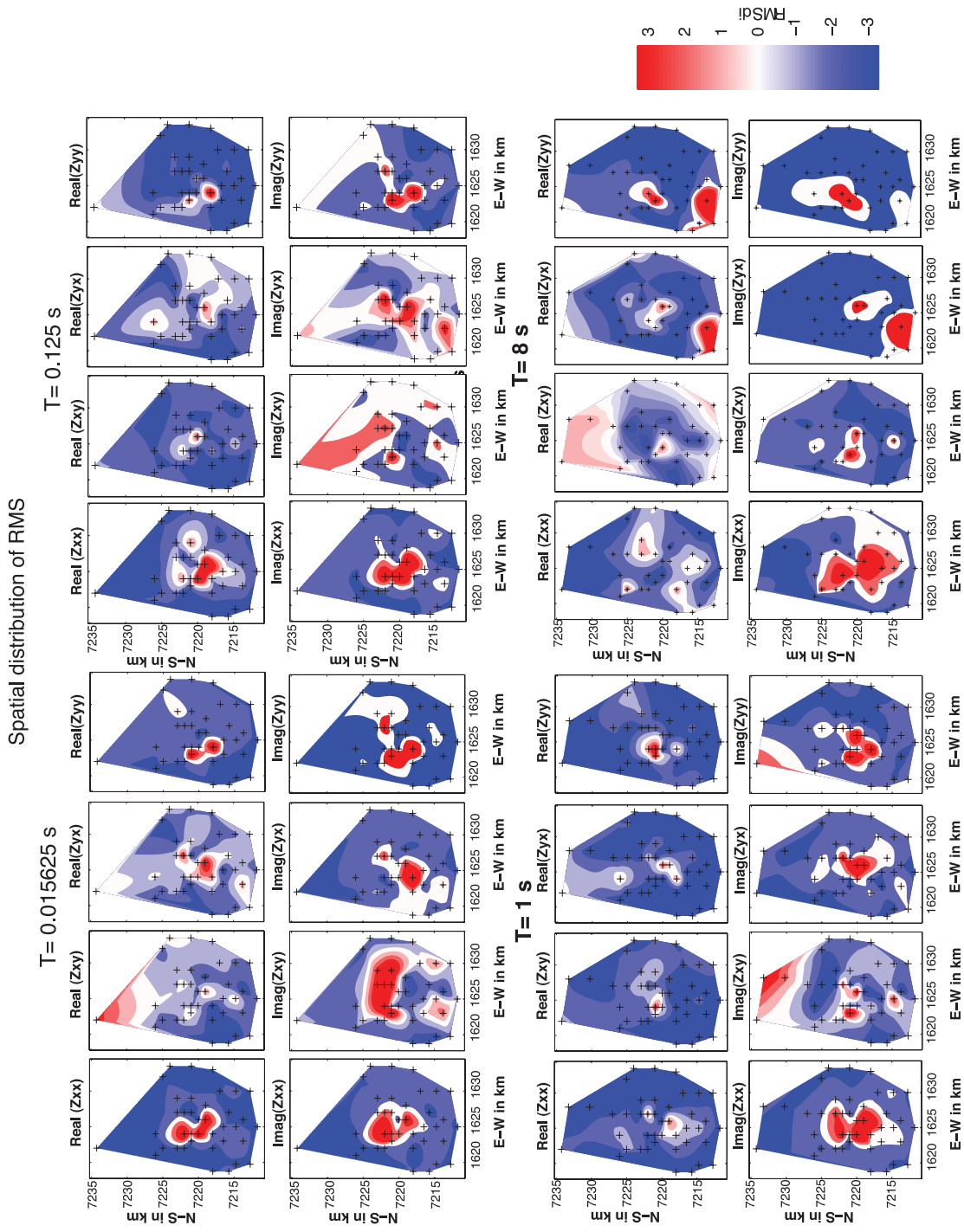
Figure 4. Spatial distribution of rms for the final model for four selected periods and all eight responses, displayed as the difference to the overall rms of 3.3 (white colour). Blue colours indicate better fit than the average, red a worse fit.
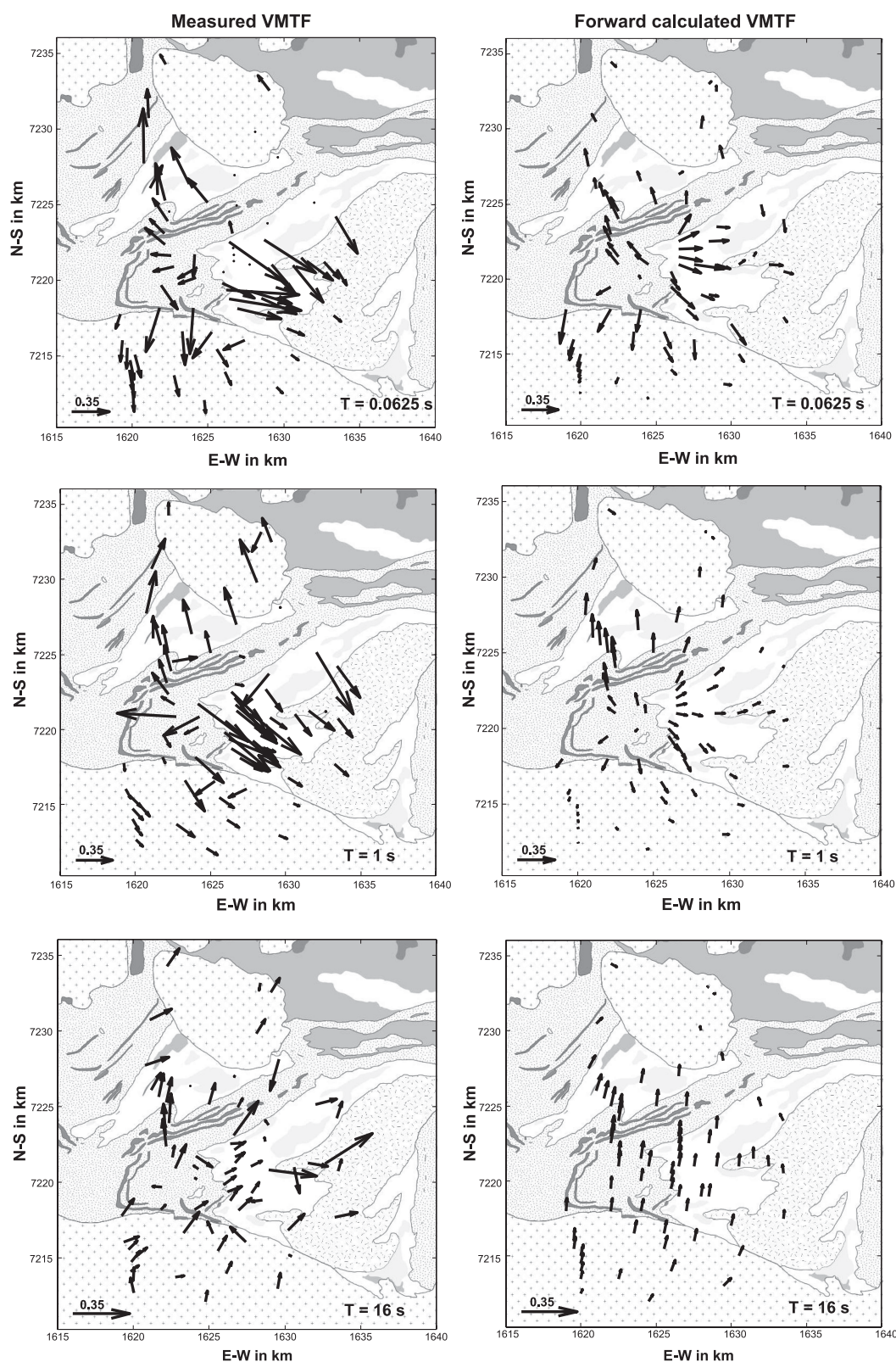
Figure 5. Real induction arrows, plotted after Wiese (1962) (pointing away from regions of electric current concentrations) for three selected frequencies 16 Hz, 1 s and 16 s. Left-hand side: measured data, right-hand side: forward response from final model. For the geological legend see Fig. 2.

periods (Fig. 5) generally exhibit a lower amplitude than the measured data. This might be caused by the regional 2-D structures, known to dominate the area (Rasmussen *et al.* 1987), which could reinforce the induction arrows on a scale that is not modelled here.

Nevertheless, we believe that the forward VMTF data lend support to the conductivity structure of the final inversion model with some strong shallow conductors in the centre of the array and a deep conductor to the south–southwest. Because the VMTF data were not included in the inversion process, this qualitative agreement between the measured and forward data supports the validity of the derived model.

4 RESULTS AND DISCUSSION

The final result of the inversion process is a smooth model with very distinctive features. The conductivities show distinct contrasts, ranging from several thousand Ohm metres in the resistive parts (features RI–III in Figs 7–11) to as low as around 1 Ωm (features CI-III). There are some agreements between the surface geology and lateral changes in conductivity that support the correlation between electrical features and lithological units.

4.1 The final resistivity model

4.1.1 Conductive structures

The most dominant features in the 3-D model are the strong conductors at various depth levels. Starting at ∼4 km in the southern part of the area is the deep conductor CI. Hübert *et al.* (2009) earlier identified it as the Skellefte crustal conductivity anomaly that was discovered by Rasmussen *et al.* (1987) with measurements east of the Kristineberg area. With the available frequency band, the electromagnetic field does not penetrate the base of the anomaly, therefore we cannot present new thickness constraints. CI vanishes towards the north and possibly towards the east, which is qualitatively confirmed by the induction arrows for periods $>10s$, that point towards northeast (see Fig. 5). Several shallow conductors (CII) appear directly at the surface in the central part of the Kristineberg area with an approximated thickness of ≈ 200 m. The insufficient spatial resolution due to the station spacing and horizontal model discretization does not allow to distinguish between actual conductivity anomalies at this depth and artefacts that were introduced by the inversion to account for galvanic distortion caused by local inhomogeneities. Nevertheless, additional information from borehole data close to site MT 104 and airborne EM data (not shown due to confidentiality) confirms the presence of black shales (with enhanced conductivity due to graphite) in the contact between metasediments and Skellefte volcanics (García Juanatey *et al.* 2012) at a depth of 200 m. Also interesting are the intermediate depth conductors (CIII) starting at ca. 1 km depth, which already occurred as a then presumably off-profile feature on the 2-D model from Profile 5 (Hübert *et al.* 2009). Their origin is unclear, but could be explained with alteration zones or ore occurrences in the metavolcanics.

4.1.2 Resistive structures

Almost the whole area is covered with electrically resistive zones of various thicknesses. Most prominent are the southern and northern resistors (RIa,b) which coincide with the surface geologic trace of the Revsund intrusions. To the south their depth is estimated to be 3–4 km underlain with the very high conductivity of CI, whereas

the northern resistor reaches to at least 5 km and is not bound by a deeper conductor. To the east, the resistor RII is mapped as a sheet like resistor whose northern boundary agrees well with the surface trace of the contact between metasediments and metavolcanics (see Fig. 7). Extending to 3 km depth in the east, it is thinning out towards the west to *ca.* 1.5 km depth. It can be associated with the Viterliden intrusion, but cannot be distinguished entirely from the metavolcanics. In the central part of Profile 5, SW of site MT13, a resistive feature (RIII) with a depth extent of less then 2 km is possibly caused by many mafic dykes in the metasediments. These also have a strong magnetic signature (*cf.* Malehmir *et al.* 2007).

4.1.3 Intermediate conductive structures

The metasediments in the absence of mafic dykes are depicted as medium conductive structures (*ca.* 30–300 Ωm, green colours in Figs 6–11). The metavolcanic rocks of the Skellefte group do not show unique electrical properties, as previously stated by García Juanatey *et al.* (2012). In zones with less alterations (e.g. in the northern segment of Profile 5) resistivities seem to be high and they cannot be easily distinguished from the metasediments or the Viterliden intrusion, whereas in the central part of the area (stations MT102–MT109) higher conductivity zones can occur.

4.2 Comparison between 2-D and 3-D inversion models

The comparison of 2-D and 3-D magnetotelluric inversion models serves two purposes: First, to assess if the 3-D inversion produces similar results in respect to required electrical features in the model along the 2-D profiles. Since it is easier to perform extensive sensitivity tests in 2-D, it is a support for the 3-D model if there is correspondence between the models and both image similar anomalies. Second, to determine the actual positioning of possible off-profile features in the 2-D sections and show the advances of using the full 3-D inversion. In 2-D it is often difficult to determine a strike direction that is valid along the whole profile and/or period range. Therefore a decoupling of TE/TM modes becomes difficult and mode mixing can occur (Becken *et al.* 2007). While using the determinant of the impedance tensor avoids defining modes, it is still possible that the projection of conductivity anomalies onto the profile section produces a distorted picture.

The comparison is sufficiently fair because from a methodological point of view both the 2-D and 3-D strategies used a similar approach: the inversion algorithms [REBOCC for 2-D (Siripunvaraporn & Egbert 2000) and WSINV3DMT for 3-D (Siripunvaraporn *et al.* 2005)] have a similar inversion scheme and model discretization (finite differences). The main difference is that the data set for the 3-D inversion was composed of the complete impedance tensor, whereas apparent resistivities and phases of the determinant average of the impedance tensor were used in the 2-D inversion. The data set for the 2-D case comprised 33 periods (128 Hz-128 s) at 10 sites on each profile, whereas in the 3-D case 12 periods (128 Hz–16 s) at 42 sites were used. To account for static shift effects due to local inhomogeneities, that is, anomalies on and off-profile in 2-D with smaller depth extent than the shallowest penetration depth, it is common practice to down-weight apparent resistivity data with a higher error floor. In the 3-D case, the inversion model should be able to represent local inhomogeneities, provided that the discretization is sufficient (Newman *et al.* 2003). Due to the smaller computational cost for the 2-D inversion, the 2-D model was discretized with a finer grid. Data sampling along a 2-D profile line has also higher
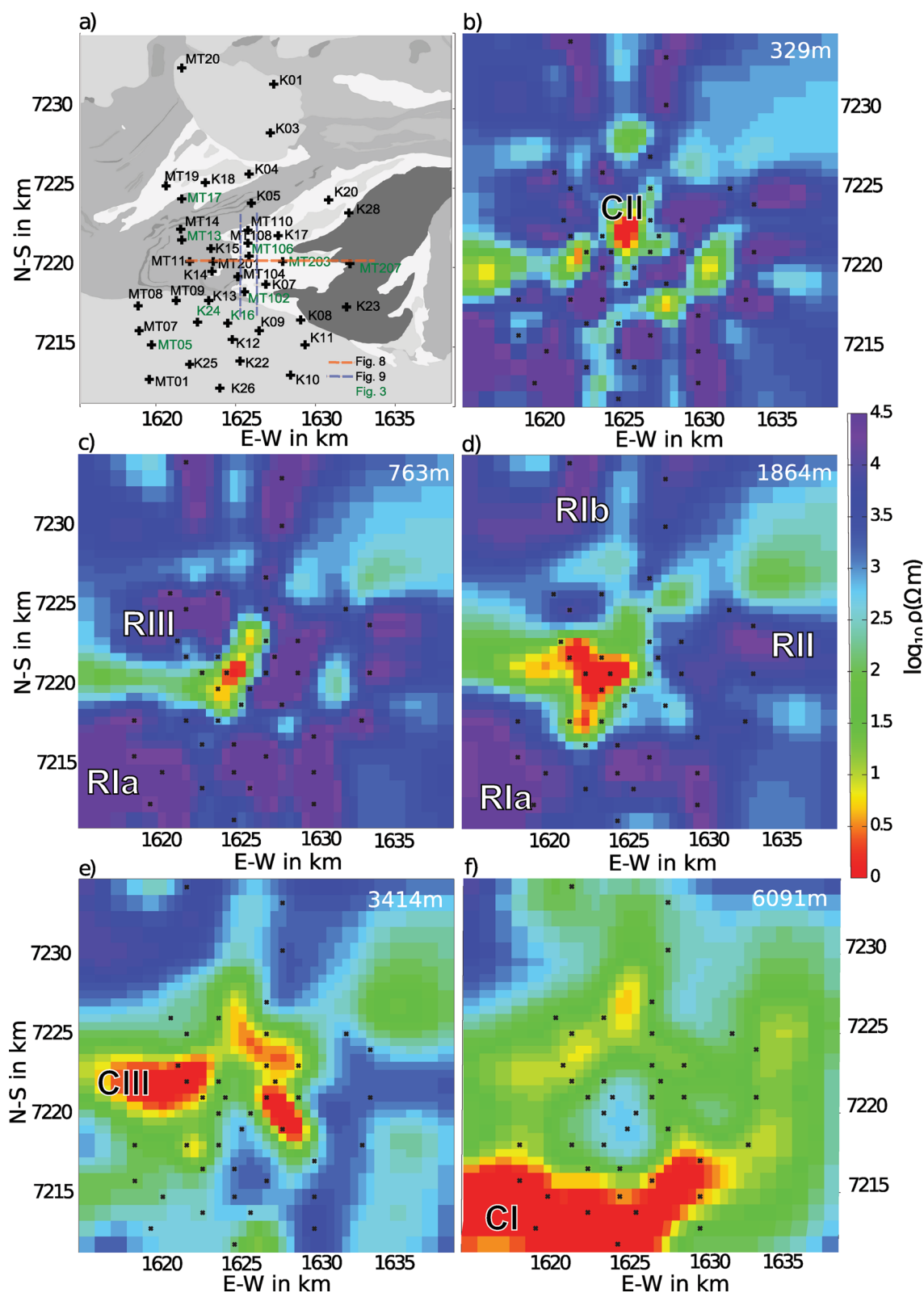
Figure 6. (a) Position of stations and slices through 3-D inversion model and profiles shown in Fig. 8+9. (b–f) Horizontal slices through the 3-D inversion model at different depth levels. The main electrical features are labelled.

coverage than in the 3-D case. Accordingly, the 3-D model has lower resolution due to the coarser grid and sparser sampling.

We compare the previous 2-D inversion models from García Juanatey *et al.* (2012) along the two central profiles (N–S and

E–W in Fig. 2) with sections through the new 3-D model. A general difference between the models is that the highest conductivities, especially for the intermediate and deep conductors, are not as extreme in the 3-D models. Resitivities well below 1 Ωm in the 2-D
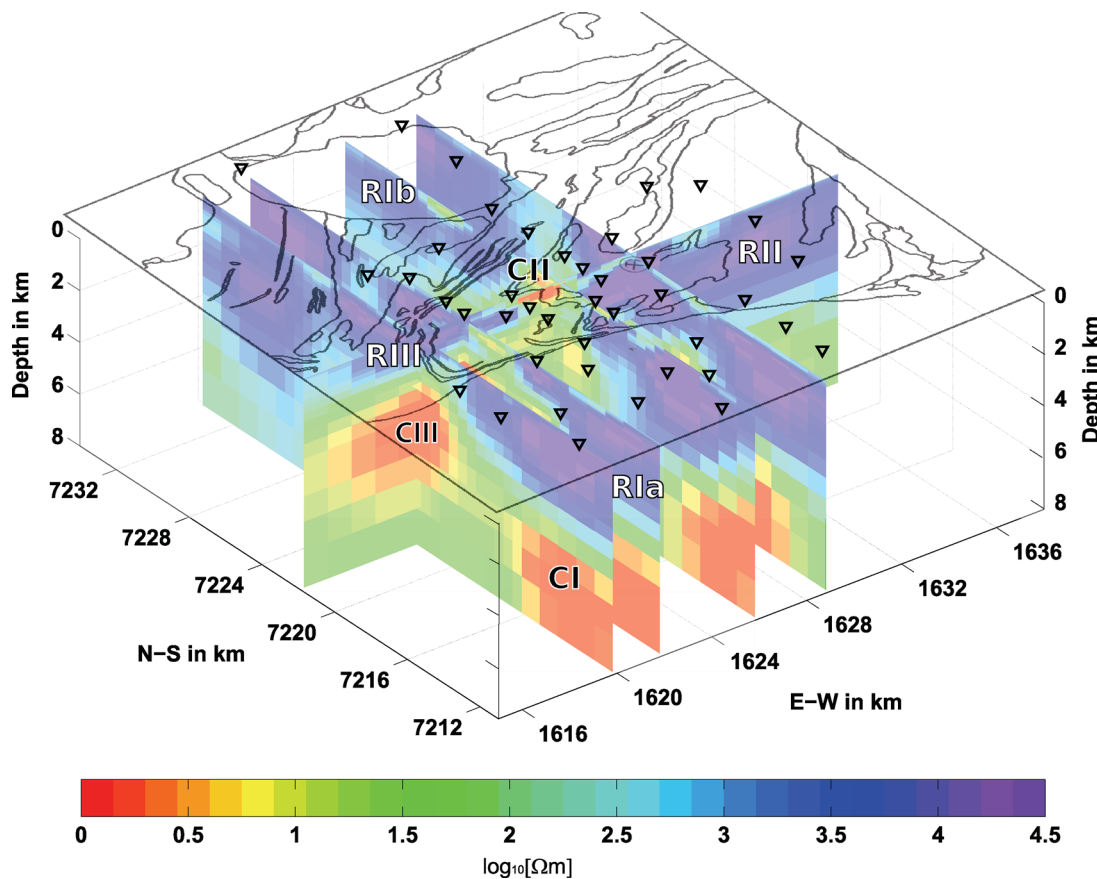
Figure 7. Slices through the 3-D conductivity model of the Kristineberg area with overlying geological map. Features: RIa+b, Revsund granite; RII, Viterliden intrusion; RIII, Mafic dykes within metasediments; CI, Skellefte crustal anomaly; CII, shale-bearing metasediments; CIII, alteration zones within the metavolcanic rocks.

case were most likely caused by 3-D effects on the phase data (Pedersen & Engels 2005).

Along the E–W Profile (Fig. 8), there is good correspondence between 2-D and 3-D results: the position and depth estimates of the intermediate conductor (CIII) and of the resistor related to the Viterliden intrusion (RII) are similar. Nevertheless, in the 3-D model there is no evidence for the deep conductor. This might be due to the more limited period range used in 3-D. On the other hand forward studies from García Juanatey *et al.* (2012) revealed that the presence of a deep off-profile conductor can effect the model and introduce ghost conductors.

Along the N–S Profile (Fig. 9) there are strong east–west variations in the resistivity distribution, therefore we compare the 2-D model with two parallel slices through the 3-D model which are 1 km apart (see Fig. 6a). The southern part of the 2-D model corresponds well with the western slice (Fig. 9, right upper panel): the position of the shallow conductor (CII) and the resistor associated with the Revsund intrusion (RIa) are very similar. The largest difference though is that the 3-D model does not depict the intermediate conductor below CII, which was already identified as a zone of less sensitivity in the 2-D model. The 3-D model places the intermediate conductor further to the east, starting at 2.5 km depth. This is a good example where the 2-D inversion projected off-profile features onto the profile line and an interpretation was difficult. With the results from 3-D inversion it is now clear that the downward smearing of the shallow conductor is an artefact.

Along Profile 5 (Hübert *et al.* 2009), the comparison (not shown) reveals very similar features, with similar depths and resistivities. Especially the position of the deep and intermediate conductors are almost identical. A sharp lateral change in resistivity coincides with the surface border between granites and metasediments. This correspondence appears to be related to the fact that the data, which had quite good quality, could be already reasonably well explained by a 2-D model.

4.3 Comparison with reflection seismic data

The combination of reflection seismics and MT has proven to be a successful joint venture in the assessment of the subsurface structure (e.g. Jones 1998; Korja *et al.* 2008; Vaittinen *et al.* 2012). Particularly, MT can image steeply dipping contrast that cannot be resolved in seismics and add information on bulk properties. In the Kristineberg area, Malehmir *et al.* (2009b) derived a geologic model based mainly on 2-D reflection seismic data and 3-D potential field modelling. Interpreted seismic sections from Malehmir *et al.* (2007) along Profiles 1 and 5 are displayed together with slices through the 3-D resistivity model in Figs 10 and 11.

Along Profile 1 (Fig. 10) there is some correlation between the lateral extension of the resistive bodies RIa and RIb. The lower boundary of the resistor associated with the Southern Revsund granite (RIa) coincides with the contact between a deeper very reflective and an overlaying less reflective zone. This is also the upper boundary of the deep conductor CI, which is a well-resolved
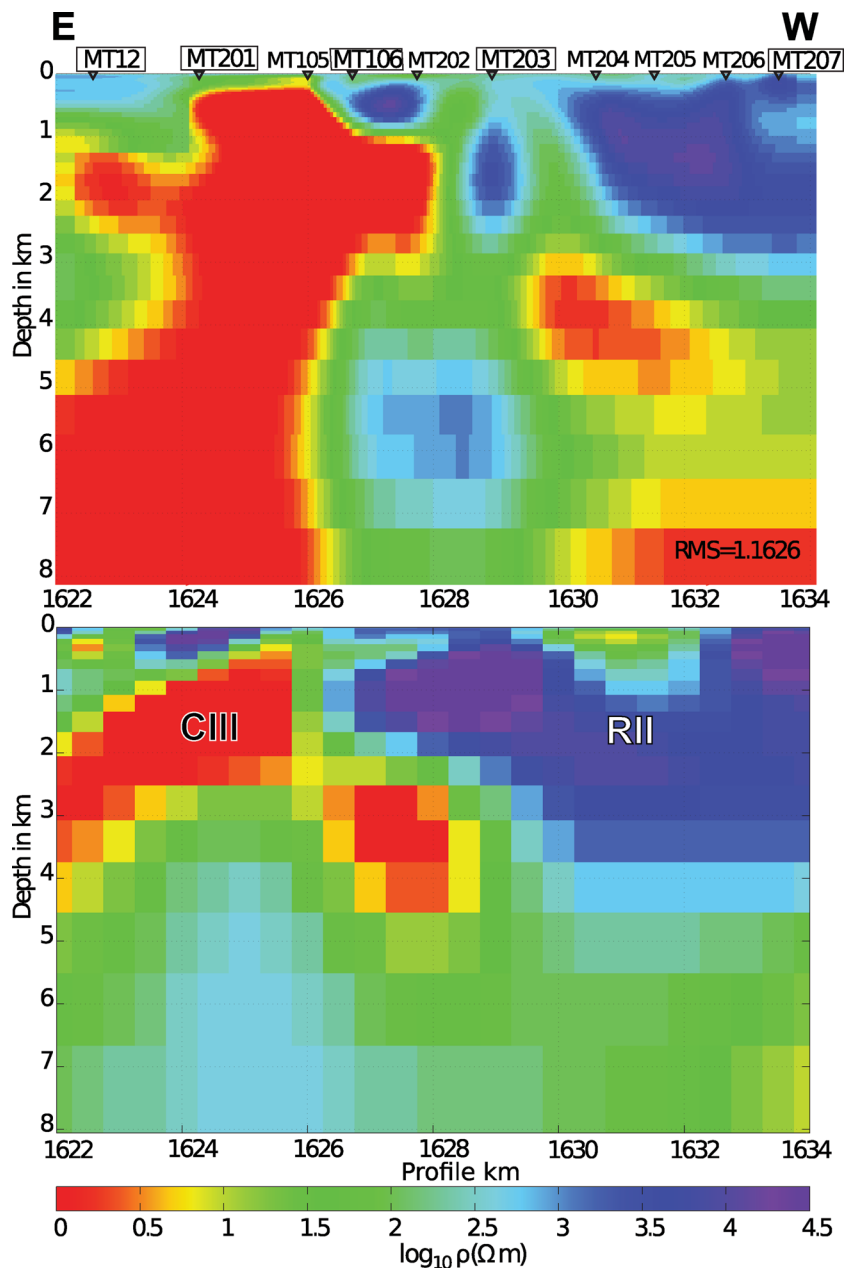
Figure 8. Comparison between 2-D (upper) and 3-D (lower) inversion models along the E–W Profile. The location of the profile line and slice can be seen in Fig. 6(a). The 2-D model is modified from García Juanatey *et al.* (2012) and coincides with the seismic reflection line on the E–W Profile (location see Fig. 2). Boxed station names indicate sites included in the 3-D inversion.

feature in the MT model. The conductor CIII at intermediate depth falls into a zone of less distinctive reflective properties. The resolution of the model is probably too low to identify the previously defined anticline that holds the Kristineberg mine (feature E in Fig. 10).

Along Profile 5 (Fig. 11) the 3-D model shows consistent correlation to the reflectivity classification in the 2-D model from the pilot study (Hübert *et al.* 2009). The lateral boundaries of resistivity features coincide with changes in reflectivity. In the southern part, the upper boundary of the deep conductor CI coincides with a north dipping package of reflectors. In the central part, the resistors RIII and RIb can now be distinguished from each other, which was not possible in the 2-D model. The former is possibly caused by the many mafic dykes within the metasediments in the southern part which also show a stronger reflectivity pattern.

5 CONCLUSIONS

The Kristineberg area in the Skellefte district, northern Sweden, has been the subject of an integrated geophysical investigation. We present a 3-D resistivity model of the area that is constructed from 3-D inversion of magnetotelluric data from 42 sites. With the inversion of the full magnetotelluric impedance tensor it is no longer necessary to make simplifying assumptions on the dimensionality of the conductivity structure. This new model supports and improves most of the earlier findings. The extension of the intrusive bodies to the south of the Kristineberg mine are resolved. The presence of a strong crustal conductivity anomaly at depths greater than 3 km is confirmed. The metasediments observed on the bedrock geological map coincide with a zone of intermediate resistivity in the MT model. Volcanic alteration zones bearing VHMS deposits are

Figure 9. Comparison between 2-D (left-hand side) and 3-D (right-hand side) inversion models along the N–S Profile. The 2-D model is modified from García Juanatey *et al.* (2012) and coincides with the seismic reflection line on the N–S Profile (location see Fig. 2). Due to the strong lateral changes we present two slices through the 3-D model, 1 km apart from each other. The location of the profile line and slices can be seen in Fig. 6(a). Boxed station names indicate sites included in the 3-D inversion.
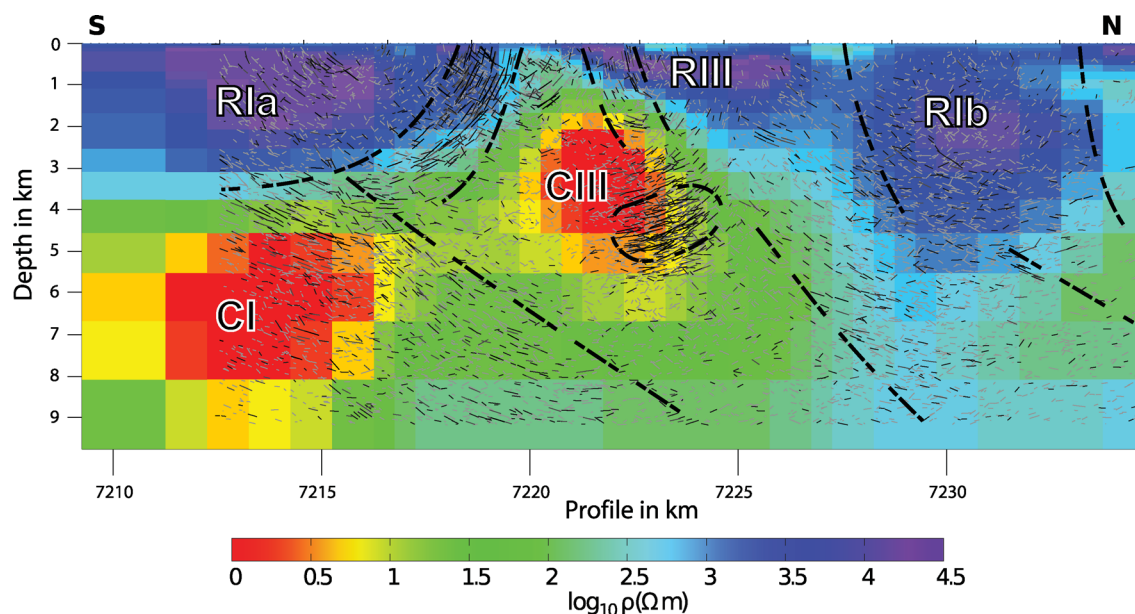

Figure 10. Section through the 3-D conductivity model along Profile 1 (location see Fig. 2), together with the migrated line drawings of seismic reflection sections from Malehmir *et al.* (2007). The dashed lines indicate interpreted lithological units from the reflection seismic study and potential field modelling. Feature E is the anticipated anticline that comprises the Kristineberg mine.

associated with the strong conductive anomalies at an intermediate depth of 1.5–2.5 km. The central part of the investigation area is characterized by several shallow strong conductivity anomalies that are most probably caused by the graphite in black shales in the contact between metasediments and metavolcanics.

Even though data quality was varying over the study area due to the presence of infrastructure, we derived a reasonable model,

that is supported by the comparison to existing 2-D inversion results along profiles and forward 3-D modelling of vertical magnetic transfer function data. The former 2-D interpretation has been revised and improved, especially the 3-D effects from the shallower conductors that were distorting the 2-D models could be better assessed. Further support comes from the integration of seismic reflection data into the interpretation that reveals good correspondence

Figure 11. Section through the 3-D conductivity model along Profile 5 (location see Fig. 2), together with migrated line drawings of seismic reflection sections from Malehmir *et al.* (2007). The dashed lines indicate interpreted lithological units from the reflection seismic study and potential field modelling.

between zones of reflectivity and the main electrical features along two profiles.

REFERENCES

Arnason, K., Eysteinsson, H. & Hersir, G.P., 2010. Joint 1D inversion of TEM and MT data and 3D inversion of MT data in the Hengill area, SW Iceland, *Geothermics,* **39**(1), 13–34.

Avdeev, D., Kuvshinov, A., Pankratov, O. & Newman, G., 2002. Three-dimensional induction logging problems, part I: an integral equation solution and model comparisons, *Geophysics,* **67**(2), 413–426.

Bauer, T., Skyttä, P., Allen, R.L. & Weihed, P., 2011. Syn-extensional faulting controlling structural inversion—insights from the Palaeoproterozoic Vargfors syncline, Skellefte mining district, Sweden, *Precamb. Res.,* **191**(3-4), 166–183.

Becken, M., Ritter, O. & Burkhardt, H., 2007. Mode separation of magnetotelluric responses in three-dimensional environments, *Geophys. J. Int.,* **172**(1), 67–86.

Bergman-Weihed, J., 1999–2000. Palaeoproterozoic deformation zones in the Skellefte and Arvidsjaur areas, northern Sweden, *Econ. Geol. Res.,* **1,** 36–395.

Bergström, U., 2001. Geochemistry and tectonic setting of volcanic units in the northern Västerbotten country, northern Sweden, *Econ. Geol. Res.,* **1**(C833), 69–92.

Billstrom, K. & Weihed, P., 1996. Age and provenance of host rocks and ores in the paleoproterozoic Skellefte district, northern Sweden, *Econ. Geol. Bull. Soc. Econ. Geol.,* **91**(6), 1054–1072.

Dehghannejad, M., Juhlin, C., Malehmir, A., Skytta, P. & Weihed, P., 2010. Reflection seismic imaging of the upper crust in the Kristineberg mining area, northern Sweden, *J. appl. Geophys.,* **71**(4), 125–136.

Farquharson, C., Oldenburg, D., Haber, E. & Shekhtman, R., 2002. An algorithm for the three-dimensional inversion of magnetotelluric data, *Proceedings of the 72nd Annual International Meeting of the Society of Exploration Geophysicists (2002),* pp. 649–652, Salt Lake City.

Gaal, G. & Gorbatshev, R., 1987. An outline of the Precambrian evolution of the Baltic Shield, *Precamb. Res.,* **35,** 15–52.

García Juanatey, M. d. l.A., Hübert, J., Tryggvason, A. & Pedersen, L.B., 2012. Imaging the Kristineberg mining area with two perpendicular magnetotelluric profiles in the Skellefte Ore District, northern Sweden, *Geophys. Prospect,* doi:10.1111/j.1365–2478.2011.01040.x.

Hautot, S., Single, R.T., Watson, J., Harrop, N., Jerram, D.A., Tarits, P., Whaler, K. & Dawes, G., 2007. 3-D magnetotelluric inversion and model validation with gravity data for the investigation of flood basalts and associated volcanic rifted margins, *Geophys. J. Int.,* **170**(3), 1418–1430.

Heise, W., Caldwell, T.G., Bibby, H.M. & Bannister, S.C., 2008. Three-dimensional modelling of magnetotelluric data from the Rotokawa geothermal field, Taupo Volcanic Zone, New Zealand, *Geophys. J. Int.,* **173,** 740–750.

Heise, W., Caldwell, T.G., Bibby, H.M. & Bennie, S.L., 2010. Three-dimensional electrical resistivity image of magma beneath an active continental rift, Taupo Volcanic Zone, New Zealand, *Geophys. Res. Lett.,* **37**(L10301), doi:10.1029/2010GL043110.

Hübert, J., Malehmir, A., Smirnow, M., Tryggvason, A. & Pedersen, L.B., 2009. MT measurements in the western part of the Paleoproterozoic Skellefte Ore District, Northern Sweden: a contribution to an integrated geophysical study, *Tectonophysics,* **475**(3-4), 493–502.

Jones, A.G., 1998. Waves of the future: superior inferences from collocated seismic and electromagnetic experiments, *Tectonophysics,* **286,** 273–298.

Kathol, B. & Weihed, P., 2005. Description to regional geological and geophysical maps of the Skellefte district and surrounding areas, *Geol. Surv. Sweden, Ser. B,* **57,** 197pp.

Korja, T., Smirnov, M., Pedersen, L.B. & Gharibi, M., 2008. Structure of the Central Scandinavian Caledonides and the underlying Precambrian basement, new constraints from magnetotellurics, *Geophys. J. Int.,* **175**(1), 55–69.

Ledo, J., Queralt, P., Marti, A. & Jones, A., 2002. Two-dimensional interpretation of three-dimensional magnetotelluric data: an example of limitations and resolution, *Geophys. J. Int.,* **150**(1), 127–139.

Malehmir, A., Tryggvason Juhlin, C., Rodriguez-Tablante, J. & Weihed, P., 2006. Seismic imaging and potential field modeling to delineate structures hosting VHMS deposits in the Skellefte Ore district, northern Sweden, *Tectonophysics,* **426**, 319–334.

Malehmir, A., Tryggvason, A., Lickorish, H. & Weihed, P., 2007. Regional structural profiles in the Western part of the Paleoproterozoic Skellefte Ore District, northern Sweden, *Pecambrian Res.,* **159**, 1–18.

Malehmir, A., Schmelzbach, C., Bongajum, E., Bellefleur, G., Juhlin, C. & Tryggvason, A., 2009a. 3D constraints on a possible deep > 2.5 km massive sulphide mineralization from 2D crooked-line seismic reflection data in the Kristineberg mining area, northern Sweden, *Tectonophysics,* **479**(3-4), 223–240.

Malehmir, A., Thunehed, H. & Tryggvason, A., 2009b. The Paleoproterozoic Kristineberg mining area, northern Sweden: results from integrated 3D geophysical and geologic modeling, and implications for targeting ore deposits, *Geophysics,* **74**(1), B9–B22.

Muñoz, G., Mateus, A., Pous, J., Heise, W., Santos, F.M. & Almeida, E., 2008. Unraveling middle-crust conductive layers in Paleozoic Orogens through 3D modeling of magnetotelluric data: the Ossa-Morena Zone case study (SW Iberian Variscides), *J. geophys. Res.-Solid Earth,* **113**(B06106), doi:10.1029/2007JB004987.

Newman, G.A. & Alumbaugh, D.L., 2000. Three-dimensional magnetotelluric inversion using non-linear conjugate gradients, *Geophys. J. Int.,* **140**(2), 410–424.

Newman, G.A., Recher, S., Tezkan, B. & Neubauer, F.M., 2003. 3D inversion of a scalar radio magnetotelluric field data set, *Geophysics,* **68**(3), 791–802.

Pedersen, L.B. & Engels, M., 2005. Routine 2D inversion of magnetotelluric data using the determinant of the impedance tensor, *Geophysics,* **70,** G31–G41.

Årebäck, H., Barret, T., Abrahamsson, S. & Fagerström, P., 2005. The Palaeoproteozoic Kristineberg VMS deposit, Skellefte district, northern Sweden, part I: geology, *Mineralium Deposita,* **40,** 351–367.

Rasmussen, T., Roberts, R. & Pedersen, L., 1987. Magnetotellurics along the Fennoscandian Long Range Profile, *Geophys. J. R. astr. Soc.,* **89,** 799–820.

Rutland, R., Kero, L., Nilsson, G. & Stolen, L., 2001. Nature of a major tectonic discontinuity in the Svecofennian province of northern Sweden, *Precamb. Res.,* **112,** 211–237.

Siripunvaraporn, W. & Egbert, G., 2000. An efficient data-subspace inversion method for 2D magnetotelluric data, *Geophysics,* **65,** 791–803.

Siripunvaraporn, W., Egbert, G., Lenbury, Y. & Uyeshima, M., 2005. Three-dimensional magnetotelluric inversion: data-space method, *Phys. Earth planet. Inter.,* **150**(1-3), 3–14.

Skyttä, P., Hermansson, T., Elming, S. & Bauer, T., 2010. Magnetic fabrics as constraints on the kinematic history of a pre-tectonic granitoid intrusion, kristineberg, northern sweden, *J. Struct. Geol.,* **32**(8), 1125–1136.

Skyttä, P., Hermansson, T., Andersson, J., Whitehouse, M. & Weihed, P., 2011. New zircon data supporting models of short-lived igneous activity at 1.89 ga in the western skellefte district, central fennoscandian shield, *Solid Earth,* **2**(2), 205–217.

Smirnov, M., 2003. Magnetotelluric data processing with a robust statistical procedure having a high breakdown point, *Geophys. J. Int.,* **152,** 1–7.

Tryggvason, A., Malehmir Juhlin, C., Rodriguez-Tablante, J. & Weihed, P., 2006. Seismic reflection investigation in the western part of the Palaeoproterozoic Skellefte Ore District, northern Sweden, *Econ. Geol.,* **101,** 1039–1054.

Vaittinen, K., Korja, T., Kaikkonen, P., Lahti, I. & Smirnov, M.Y., 2012. High-resolution magnetotelluric studies of the Archaean-Proterozoic border zone in the Fennoscandian Shield, Finland, *Geophys. J. Int.,* **188**(3), 908–924.

Weihed, P., Bergman, J. & Bergström, U., 1992. Metallogeny and tectonic evolution of the Early Proterozoic Skellefte District, northern Sweden, *Precamb. Res.,* **58,** 143–167.

Weihed, P., Billström, K., Persson, P.-O. & Bergman-Weihed, J., 2002. Relationship between 1.90–1.85 Ga accretionary processes and 1.82-1.80 Ga oblique subduction at the Karelian craton margin, Fennoscandian Shield, *Geologiska Föreningens I Stockholm Förhandlingar,* **124,** 163–180.

Wiese, H., 1962. Geomagnetische Tiefentellurik Teil II: die Streichrichtung der Untergrundstrukturen des elektrischen Widerstands, erschlossen aus geomagnetischen Variationen, *PAGEOPH,* pp. 83–103.

Zhdanov, M.S., Green, A., Gribenko, A. & Cuma, M., 2010. Large-scale three-dimensional inversion of earthscope mt data using the integral equation method, *Phys. Solid Earth,* **46,** 670–678.